



NRL/MR/6750--14-9519

On Improving Impedance Probe Plasma Potential Measurements

DAVID N. WALKER

*Sotera Defense Solutions, Inc.
Herndon, Virginia*

DAVID D. BLACKWELL

RICHARD F. FERNSLER

WILLIAM E. AMATUCCI

*Charged Particle Physics Branch
Plasma Physics Division*

February 21, 2014

Approved for public release; distribution is unlimited.

REPORT DOCUMENTATION PAGE				Form Approved OMB No. 0704-0188	
Public reporting burden for this collection of information is estimated to average 1 hour per response, including the time for reviewing instructions, searching existing data sources, gathering and maintaining the data needed, and completing and reviewing this collection of information. Send comments regarding this burden estimate or any other aspect of this collection of information, including suggestions for reducing this burden to Department of Defense, Washington Headquarters Services, Directorate for Information Operations and Reports (0704-0188), 1215 Jefferson Davis Highway, Suite 1204, Arlington, VA 22202-4302. Respondents should be aware that notwithstanding any other provision of law, no person shall be subject to any penalty for failing to comply with a collection of information if it does not display a currently valid OMB control number. PLEASE DO NOT RETURN YOUR FORM TO THE ABOVE ADDRESS.					
1. REPORT DATE (DD-MM-YYYY) 21-02-2014		2. REPORT TYPE Memorandum Report		3. DATES COVERED (From - To)	
4. TITLE AND SUBTITLE On Improving Impedance Probe Plasma Potential Measurements				5a. CONTRACT NUMBER	
				5b. GRANT NUMBER	
				5c. PROGRAM ELEMENT NUMBER	
6. AUTHOR(S) David N. Walker,* David D. Blackwell, Richard F. Fernsler, and William E. Amatucci				5d. PROJECT NUMBER 67-4988-04	
				5e. TASK NUMBER	
				5f. WORK UNIT NUMBER	
7. PERFORMING ORGANIZATION NAME(S) AND ADDRESS(ES) Naval Research Laboratory 4555 Overlook Avenue, SW Washington, DC 20375-5320				8. PERFORMING ORGANIZATION REPORT NUMBER NRL/MR/6750--14-9519	
9. SPONSORING / MONITORING AGENCY NAME(S) AND ADDRESS(ES) Office of Naval Research One Liberty Center 875 North Randolph Street, Suite 1425 Arlington, VA 22203-1995				10. SPONSOR / MONITOR'S ACRONYM(S) ONR	
				11. SPONSOR / MONITOR'S REPORT NUMBER(S)	
12. DISTRIBUTION / AVAILABILITY STATEMENT Approved for public release; distribution is unlimited.					
13. SUPPLEMENTARY NOTES *Sotera Defense Solutions, Inc., Herndon, VA 20171					
14. ABSTRACT In earlier works we used spheres of various sizes as impedance probes in demonstrating a method of determining plasma potential ϕ_p , when the probe radius is much larger than the Debye length, λ_D . The basis of the method in those works relies on applying a small amplitude signal of fixed frequency to a probe in a plasma and measuring the complex reflection coefficient, Γ , for varying probe bias, V_b . For a given frequency, $\text{Re}(Z_{ac})$ (the real part of the complex plasma impedance determined from Γ) is plotted versus V_b , and a minimum predicted by theory occurs at ϕ_p for a large range of electron density, n_e . However, the frequency range of the applied signal is restricted as we briefly review in this paper. As n_e decreases, or the sheath grows to the order of the probe radius, the frequency range becomes even more restrictive and, in addition, the minimum in $\text{Re}(Z_{ac})$ in experimental data at $V_b = \phi_p$ becomes difficult to discern.					
15. SUBJECT TERMS Plasma physics Impedance probes Plasma potential determination Plasma diagnostics Network analyzer					
16. SECURITY CLASSIFICATION OF:			17. LIMITATION OF ABSTRACT Unclassified Unlimited	18. NUMBER OF PAGES 19	19a. NAME OF RESPONSIBLE PERSON David D. Blackwell
a. REPORT Unclassified Unlimited	b. ABSTRACT Unclassified Unlimited	c. THIS PAGE Unclassified Unlimited			19b. TELEPHONE NUMBER (include area code) (202) 767-6781

TABLE OF CONTENTS

<i>I</i>	<i>Introduction.....</i>	1
<i>II</i>	<i>Further indicators of plasma potential.....</i>	4
	<i>II.1 The plasma impedance Z_{ac}.....</i>	4
	<i>II.2 The reflection coefficient, Γ, and its derivative.....</i>	5
	<i>II.3 $\text{Im}(Z_{ac})$ and its derivative.....</i>	5
<i>III</i>	<i>$\text{Re}(Z_{ac})$ vs V_{bias} as a function of frequency and electron density.....</i>	6
<i>IV</i>	<i>Experimental results for different probe geometries.....</i>	6
	<i>IV.1 Spherical probe.....</i>	7
	<i>IV.2 Cylindrical probe.....</i>	10
	<i>IV.3 Disk probe.....</i>	11
	<i>IV.4 Comparison of disk probe and sphere.....</i>	12
<i>V.</i>	<i>Appendix A</i>	13
<i>VI.</i>	<i>Summary.....</i>	15
<i>VII.</i>	<i>References.....</i>	16

On Improving Impedance Probe Plasma Potential Measurements

I. Introduction

In earlier works we used spheres of various sizes as impedance probes in demonstrating a method of determining plasma potential, ϕ_p , when the probe radius is much larger than the Debye length, λ_D . The basis of the method in those works¹⁻⁴ relies on applying a small amplitude signal of fixed frequency to a probe in a plasma and measuring the complex reflection coefficient, Γ , for varying probe bias, V_b . For a given frequency, $\text{Re}(Z_{ac})$ (the real part of the complex plasma impedance determined from Γ) is plotted versus V_b , and a minimum predicted by theory occurs at ϕ_p for a large range of electron density, n_e ³. However, the frequency range of the applied signal is restricted as we briefly review in this paper. As n_e decreases, or the sheath grows to the order of the probe radius, the frequency range becomes even more restrictive and, in addition, the minimum in $\text{Re}(Z_{ac})$ in experimental data at $V_b = \phi_p$ becomes difficult to discern. Here, we extend the range of application of the technique by including further measures useful in isolating the inflection point indicative of ϕ_p . These measures extend the analysis by; (1) incorporating Γ into the algorithm to search for the minimum at $V_b = \phi_p$, (2) using not only the first derivative of $\text{Re}(Z_{ac})$, but also that of $\text{Im}(Z_{ac})$ with respect to V_b in addition to, (3) using the second derivatives of both. With these additional indicators, both the minimum and the frequency restriction on determining ϕ_p become clearer as we demonstrate in the data. In the past, we compared results to a Langmuir probe sweep determination of ϕ_p and in the present case we extend the comparison to include an emissive probe also. The Appendix addresses the current state of the theory with regard to the experimentally observed maximum in $\text{Im}(Z_{ac})$. We concentrate mostly on spherical probe data in demonstrating the use of the new indicators although we present limited data for a cylinder⁴ and a disk for comparison purposes.

The measurement of plasma potential as done historically with conventional Langmuir probes⁵⁻⁸ typically involves either a curve-fitting technique based on the intersection of straight line fits to the electron saturation and electron-retarding field regions of the probe characteristic; or a measurement of floating potential accompanied by the assumption that the difference between floating potential and plasma potential is simply T_e/e ^{5,6}. These methods are based on the assumption of a collisionless, stationary Maxwellian plasma and are seen to work well in non-flowing plasmas of sufficient density. However, as plasma density decreases, the characteristic IV trace becomes more rounded and the inflection point, or “knee”, argued to be plasma potential, is more

difficult to discern. When plasma sheaths are small with respect to probe size, the probe surface collecting area is very nearly the same as that of the sheath with often very little change in the sheath radius as the applied voltage is increased. The current collected in this area (electron saturation current) is that due to random electron current and should therefore also show little change as the voltage increases. This should be true independent of probe geometry. However, as the sheath becomes larger, orbital motions of collected electrons (Orbital Motion Limited (OML) theory) must be considered and current collection can increase in the electron saturation regime over its thin sheath limit. In addition, current collection dependence on applied bias voltage has been shown to vary as a function of probe geometry; for example, the IV characteristic of a plane probe exhibits a more distinct change of slope than a cylinder which in turn has a more distinct break than a sphere in this regime.⁵ This is further complicated by an increasing T_e which expands the slope of the IV trace in the electron retarding area. In addition, unless T_e is measured by some other means, it is more difficult to determine.

In difficult cases such as mentioned above, the inflection point can be more confidently identified if the derivative is included in the analysis along with the function. This is a commonly used technique in locating, for example, a local extremum of a function of one variable by using the derivative with respect to the independent variable. This can apply to the Langmuir probe IV trace where the derivative, dI_e/dV_b , is used in combination with I_e where I_e is electron current collected by the probe and V_b is the applied probe bias. We demonstrate in Fig (1) for a small cylindrical Langmuir probe that the derivative gives a sharper definition of the “knee” than the function alone and therefore aids in this determination. There are often more serious noise issues than seen in this example. In many of these cases applying filtering suppresses random noise and hence the effect of the noise on the derivative. The figure displays the unfiltered IV characteristic, Fig 1(a), and its derivative trace , Fig 1(b), in the absence of an external magnetic field. The plasma conditions are for an electron density, $n_e = 4.5 \times 10^7 \text{ cm}^{-3}$, and temperature, $T_e = 2.4 \text{ eV}$. The neutral gas is argon at a pressure of $P_N = 2 \times 10^{-4} \text{ Torr}$. It is easier to determine plasma potential, ϕ_p , with the derivative trace accompanying the IV characteristic than with the IV trace alone.

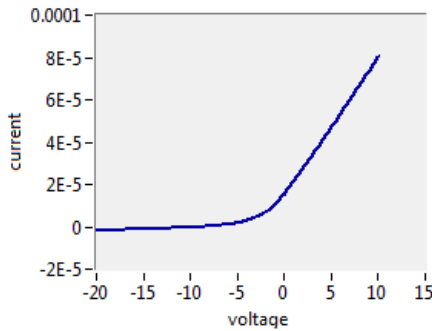


Figure 1(a)

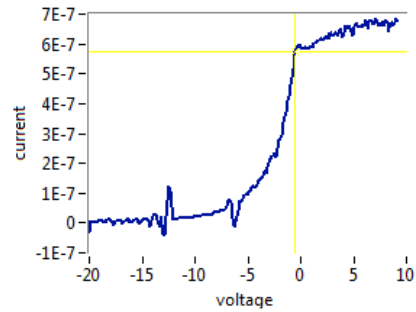


Figure 1(b)

The same idea is useful for the impedance probe algorithm developed in earlier work. In this case, when the real part of the plasma impedance, $\text{Re}(Z_{ac})$, is plotted

versus V_b for a given applied small signal ac frequency, a minimum is predicted to occur at plasma potential, ϕ_p .³ In analogy to the case of the Langmuir probe above, the position of the minimum can be isolated more easily by using $d\text{Re}(Z_{ac})/dV_b$ in conjunction with $\text{Re}(Z_{ac})$. However, as we review in this work, since

$$\text{Re}(Z_{ac}) \simeq R_{ac} \simeq \left(\frac{dI_e}{dV_b}\right)^{-1}, \quad (1)$$

where R_{ac} is the ac resistance of the plasma, the inverse slope, $(dI_e/dV_b)^{-1}$, is plotted vs V_b (instead of I_e in the Langmuir probe IV characteristic analysis). Moreover the derivative,

$$\frac{dR_{ac}}{dV_b} = -\left(\frac{dI_e}{dV_b}\right)^{-2} \frac{d^2 I_e}{dV_b^2} = -R_{ac}^2 \frac{d^2 I_e}{dV_b^2}, \quad (2)$$

or, dR_{ac}/dV_b is directly proportional to $d^2 I_e/dV_b^2$ and hence ultimately to the determination of the electron density distribution function.³

In addition to using the extended analysis of $\text{Re}(Z_{ac})$ data described above, $\text{Im}(Z_{ac})$ is also available from the basic reflection coefficient, Γ . Values of reflection coefficient Γ are obtained by measuring the complex voltage V_1 at the network analyzer port where the cable ending with the probe is connected. The magnitude and phase of V_1 are compared to the internal voltage source through a simple voltage divider circuit shown in Figure 2:

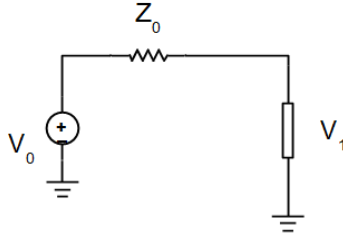


Figure 2

The complex reflection coefficient is Γ defined as,

$$\Gamma = \frac{2V_1}{V_0} - 1 \quad (3)$$

where Z_0 is the internal input impedance of the network analyzer. And from Eq. (3),

$$\Gamma = \frac{Z - Z_0}{Z + Z_0} = \frac{(\text{Re } Z - Z_0) + i \text{Im } Z}{(\text{Re } Z + Z_0) + i \text{Im } Z} \quad (4)$$

where the network analyzer input impedance, Z_0 , is 50 Ω . We will demonstrate that Γ and its first derivative may also be included in a measurement set along with $\text{Im}(Z_{ac})$ with similar considerations as with $\text{Re}(Z_{ac})$ outlined above.

A difficulty in the measurement of Γ occurs for low plasma density, in which case $Z_1 \gg Z_0$, $V_1 \approx V_0$ and $\Gamma \approx 1$. Under these conditions small calibration errors become more significant and the derived values of Z become more prone to distortions. As an example of this we plot $\text{Re } \Gamma$ vs V_b for a cylindrical probe for three different densities in Figure 3(c). In these three runs the analyzer frequency was fixed at 1 MHz. The figure demonstrates the effect of a decreasing density (increasing resistance) on the ability of the analyzer to detect magnitude differences in Γ from which $\text{Re}(Z_{ac})$ and $\text{Im}(Z_{ac})$ are calculated *i.e.*, whereas there is a 0.1% variation in $\text{Re } \Gamma$ for the highest density, this variation has fallen to an almost undetectable level with approximately a 50% variation in density.

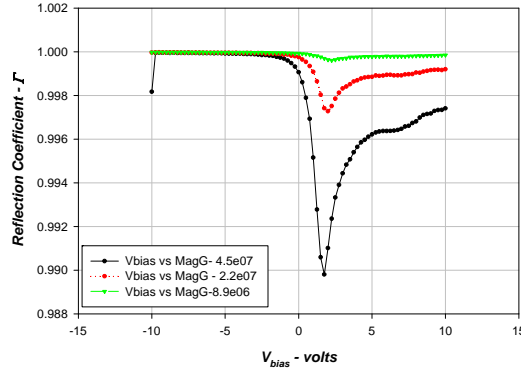


Figure 3

II. Further indicators of plasma potential

II.1 The Plasma Impedance, Z

As reviewed from earlier work³ in Appendix A, we are able to obtain expressions for both $\text{Re}(Z_{ac})$, $\text{Im}(Z_{ac})$ in the frequency range applicable to the model. In that work,

$$\text{Re}(Z_{ac}) = \frac{R_{ac}}{1 + (\omega C_s R_{ac})^2}, \quad (5)$$

$$\text{Im}(Z_{ac}) = \frac{\omega L_p + \omega R_{ac}^2 C_s (\omega^2 L_p C_s - 1)}{1 + (\omega R_{ac} C_s)^2} \quad (6)$$

Using the conditions that $(\omega R_{ac} C_s)^2 \ll 1$ and $\omega^2 L_p C_s \ll 1$ we have,

$$\text{Im}(Z_{ac}) \approx \omega L_p - \omega R_{ac}^2 C_{ac} \quad (7)$$

$$\text{and,} \quad \text{Re}(Z_{ac}) \approx R_{ac} \quad (8)$$

where $L_p \sim 1 \mu\text{H}$, $C_s \sim 1 \text{ pF}$ and $\omega \sim 1 \text{ MHz}$.

II.2 The Reflection Coefficient and its derivative

The reflection coefficient, Γ , of Eq (4), which is returned by the network analyzer, is expanded as,

$$\Gamma = \frac{\text{Re}(Z_{ac})^2 + \text{Im}(Z_{ac})^2 - Z_0^2 + 2iZ_0^2 \text{Im}(Z_{ac})}{(\text{Re}(Z_{ac}) + Z_0)^2 + \text{Im}(Z_{ac})^2} \quad (9)$$

with,

$$\text{Re} \Gamma = \frac{\text{Re}(Z_{ac})^2 (1 - (\frac{Z_0}{\text{Re}(Z_{ac})})^2) + \text{Im}(Z_{ac})^2}{\text{Re}(Z_{ac})^2 (1 + (\frac{Z_0}{\text{Re}(Z_{ac})})^2) + \text{Im}(Z_{ac})^2} \quad (10)$$

and,

$$\text{Im} \Gamma \simeq \frac{-2 \text{Im}(Z_{ac})}{\text{Re}(Z_{ac})^2 + \text{Im}(Z_{ac})^2}. \quad (11)$$

At plasma potential in the frequency range we consider ($\omega \ll \omega_{p0}$), we ignore $\text{Im}(Z_{ac})$ as it is much less than $\text{Re}(Z_{ac})$. Eq. (10) then becomes upon expansion approximately,

$$\text{Re} \Gamma = \frac{(1 - (\frac{Z_0}{\text{Re}(Z_{ac})})^2)}{(1 + (\frac{Z_0}{\text{Re}(Z_{ac})})^2)} \simeq 1 - \frac{2Z_0}{\text{Re}(Z_{ac})}. \quad (12)$$

In this form $|\Gamma|$ is seen to reach a minimum along with $\text{Re}(Z_{ac}) \approx R_{ac}$ at plasma potential, or,

$$\left. \frac{d|\Gamma|}{dV_b} \right|_{\varphi_p} = \frac{d \text{Re} \Gamma}{dV_b} = \frac{-2Z_0}{\text{Re}(Z_{ac})^2} \frac{d \text{Re}(Z_{ac})}{dV_b} \simeq 0. \quad (13)$$

II.3 $\text{Im}(Z_{ac})$ and its derivative

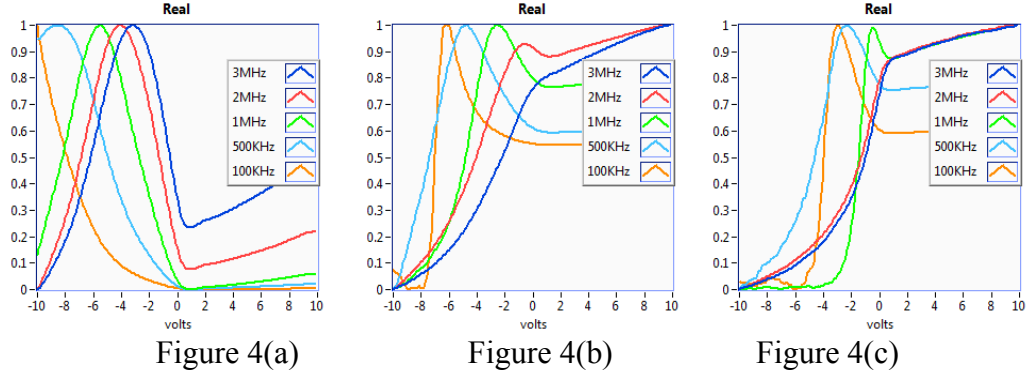
Eq. (7) gives the form of $\text{Im}(Z_{ac})$ under our frequency restrictions. The partial derivative with respect to V_b at φ_p becomes,

$$\left. \frac{\partial \text{Im}(Z_{ac})}{\partial V_b} \right|_{V_b=\varphi_p} \simeq \left(\omega \frac{\partial L_p}{\partial V_b} - \omega R_{ac}^2 C_s \left(\frac{2}{R_{ac}} \frac{\partial R_{ac}}{\partial V_b} + \frac{1}{C_s} \frac{\partial C_s}{\partial V_b} \right) \right) \bigg|_{V_b=\varphi_p} \quad (14)$$

We further analyze portions of this expression in the Appendix. Note however that since we have shown earlier that $\partial R_{ac}/\partial V_b \approx 0$ at plasma potential, under the conditions outlined, we have another indicator of plasma potential if the remaining two contributions to this expression can also be shown to be negligible. Although this is not immediately obtainable with the current theory, data below show that $\text{Im}(Z_{ac})$ reaches a maximum at plasma potential (or very close to it) and therefore that the derivative of Eq. 14 is zero as observed in the experiments.

III. $\text{Re}(Z_{ac})$ vs V_{bias} as a function of frequency and electron density

As a general introduction to the data, and as a review of earlier experimental and theoretical conclusions, we show in Figures 4(a) – 4(c) the applied frequency and electron density dependence of the minimum in $\text{Re}(Z_{ac})$ at plasma potential for a spherical probe ($r_p = 1.5$ inches). The Figure shows smoothed experimental data for $\text{Re}(Z_{ac})$ plotted vs applied bias voltage, V_b , for different applied frequencies ranging from 100 kHz to 3 MHz for three different densities in decreasing order: Figure 4(a) - $n_e = 1.7 \times 10^7 \text{ cm}^{-3}$ ($f_{pe} \approx 37 \text{ MHz}$), Figure 4(b) - $n_e = 2.7 \times 10^6 \text{ cm}^{-3}$ ($f_{pe} \approx 15 \text{ MHz}$), Figure 4(c) - $n_e = 7.6 \times 10^5 \text{ cm}^{-3}$ ($f_{pe} \approx 8 \text{ MHz}$). The figures are normalized to emphasize the curve shape as plasma density decreases.



Note that the minima in the curves near plasma potential ($V_b = \phi_p \approx 1$ volt) at a given density vary with applied frequency. Earlier work places an upper limit on the applied frequency which is approximately that $f \leq f_{pe}/3$. In Figure 4(c) the highest frequency, 3 MHz, does not meet this requirement and the next highest, 2 MHz, only marginally. For these two curves, no minimum is discernible. Also, in Figure 4(b) the highest frequency, 3 MHz, shows no indication of a minimum. In Figure 4(a) with the highest density, and a much higher plasma frequency, all curves tend to show a minimum at or near plasma potential. The data then are generally consistent with the theoretical requirement that lower density requires lower applied frequency.³ It is not always clear in some of the lower frequencies (100 kHz, 500 kHz) where the minimum lies and that is an issue we address in part here in terms of using first derivatives as covered in the Introduction. We also point out that not only are the minima a function of density and applied frequency, but also probe size is an important issue since the requirement of a thin sheath with respect to r_p is the basis of much of the theoretical effort.

IV. Experimental results for different rf probe geometries

As a brief review of the basis of the plots below, recall that the dc electron current collected by a probe in the absence of a magnetic field is $I_e = A_p e n_p (T_e / 2\pi m_e)^{1/2}$ where e is electron charge, m_e is electron mass, and T_e is electron temperature, with A_p the probe collection area. For Maxwellian electrons, $n_p = n \exp(V_p - \phi_p) / T_e$ and so at low frequency from Eq. (1) above, the resistive component of the ac impedance, R_{ac} , of a probe biased to plasma potential, ϕ_p , is (in Gaussian units),

$$\text{Re}(Z_{ac})|_{V_{bias}=\phi_p} \simeq R_{ac}(\phi_p) \equiv \left(\frac{dI_e}{dV_{bias}} \right)^{-1} \bigg|_{V_{bias}=\phi_p} = \frac{\sqrt{2\pi m_e T_e}}{e^2 n_p A_p} \quad (15)$$

The data are for three different probe geometries and a number of fixed frequencies and were gotten through measurement of the small-signal ac. We concentrate primarily on a spherical probe insofar as demonstrating the use of Γ and $\text{Im}(Z_{ac})$. As in all past work, and that presented here, a network analyzer is used to obtain the reflection coefficient from which the real and imaginary parts of the impedance are determined. Eq. (13) relates the derivative of the reflection coefficient, Γ , to that of the derivative of $\text{Re}(Z_{ac})$ and in particular shows that it goes to zero along with $\partial \text{Re}(Z_{ac}) / \partial V_b$. Further, we note in reference to ongoing work outlined in Appendix A, Eq. (7) relates $\text{Im}(Z_{ac})$ to R_{ac} and the derivative as covered above in Eq. 14. The plots of these quantities, from which plasma potential is obtained are shown below. We mention in passing that plots of $\text{Re}(Z_{ac})$ are used as the primary reference when constructing $f(\epsilon)$.³

IV.1 Spherical Probe

For these experiments we used as a probe an aluminum sphere of radius $r = 3.8$ cm which is connected to an HP8735D Network Analyzer through 50 Ω coaxial cable which provides the driving signal. The connections as described above for the cylinder were the same and only the probe itself was changed.

Figures 5(a) and 5(b) show plots of $\text{Re}(Z_{ac})$ and $\text{Im}(Z_{ac})$ vs V_{bias} but at varying ac frequency at a fixed density of $n_e = 3.8 \times 10^7 \text{ cm}^{-3}$. There is once again a minimum seen in $\text{Re}(Z_{ac})$ at plasma potential and a maximum in $\text{Im}(Z_{ac})$. At the lowest frequency of 100 kHz there appears a shift whose origin and dependence on frequency is not understood at this time.

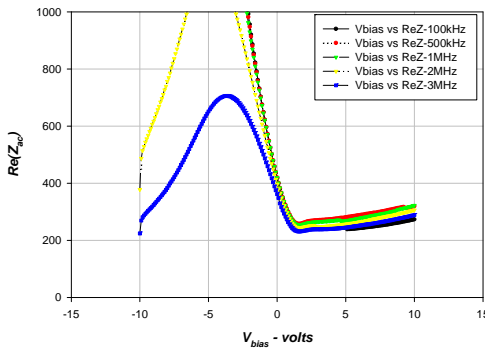


Figure 5(a)

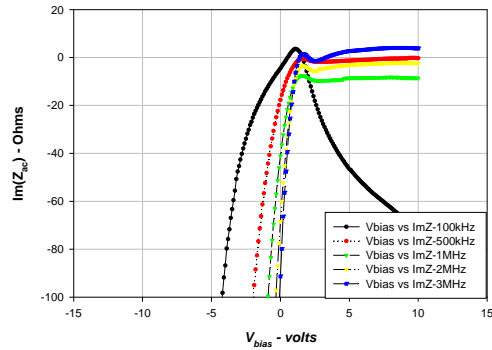


Figure 5(b)

Figures 6(a) through 6(f) are contour plots showing the magnitude of Γ and the first derivative, $d\Gamma/dV_b$, versus V_b for varying frequency for three separate densities: Figure 6(a,b) $n_e = 2 \times 10^7 \text{ cm}^{-3}$, Figure 6(c,d) $n_e = 7.7 \times 10^6 \text{ cm}^{-3}$, Figure 6(e,f) $n_e = 1 \times 10^6 \text{ cm}^{-3}$. These figures demonstrate in a single plot both the effect of varying density and frequency of the transmitted signal. In addition they are meant to stress the utility of

the derivative plots when little vague information is available from $\text{Re}(Z_{ac})$. The figures demonstrate a gradual loss of information about the plasma potential that occurs with increasing frequency as density decreases and how the additional information provided by the first derivative ameliorates this to some degree. In Figures 6(a,b) and 6(c,d) the plasma potential is near zero whereas in Figures 6(e,f) it is near -1 V. (These values are consistent with Langmuir probe results in addition to emissive probe results.) For the highest density of Figure 6(a,b) plasma potential can be more easily determined for a wide range of applied frequencies although it tends to drift as a function of frequency; for Figure 6(e,f) the frequency range is restricted to less than about 3MHz in Figure 6(e), and higher in Figure 6(f) demonstrating, as in all of the derivative plots, additional information that is not obvious from the plots of the Γ alone. (We stress that the derivative plots indicate plasma potential by going to zero as is consistent with the arguments leading to Eq (13) *i.e.*, the derivative goes to zero while the function Γ goes to a minimum)

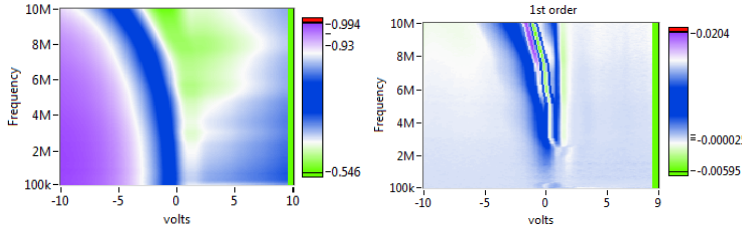


Figure 6(a)

Figure 6(b)

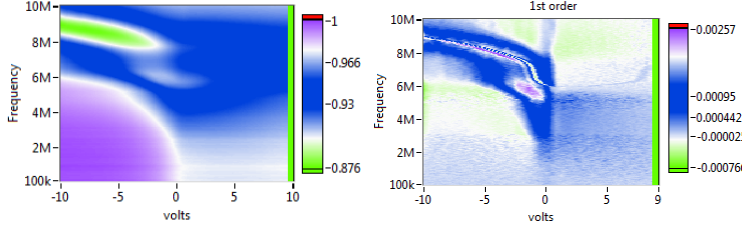


Figure 6(c)

Figure 6(d)

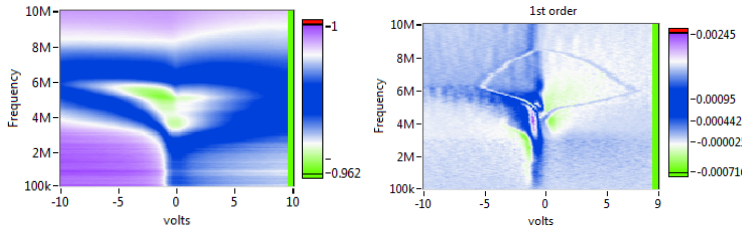


Figure 6(e)

Figure 6(f)

As a further and alternate view of the effect of both density and applied frequency on the determination of plasma potential, we present the 3-dimensional surface plots Figures

7(a) through 7(f). These are surface plots of Γ with the first derivative as above. The low ridge on the surface plot and the straight edge on the contour plots to the right are indicative of the approximate potential. The density varies as shown. Although all of the figures show this behavior to some degree, for the higher densities it is more easily isolated.

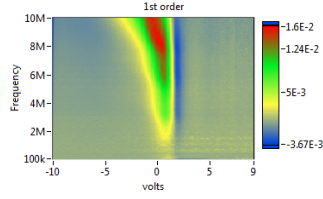
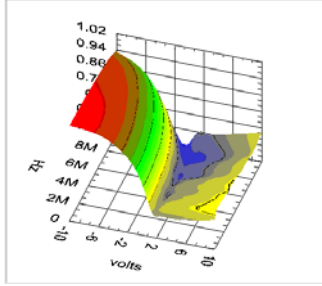


Figure 7(a)- $n_e = 3.6 - 4.4 \times 10^7 \text{ cm}^{-3}$

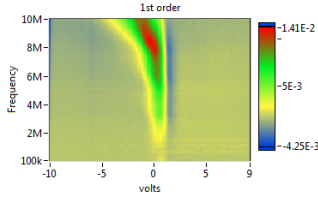
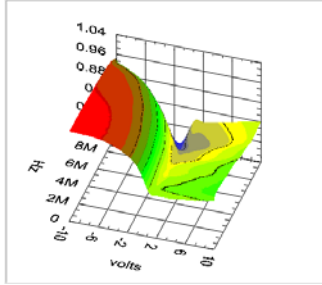


Figure 7(b)- $n_e = 2 \times 10^7 \text{ cm}^{-3}$

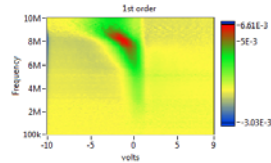
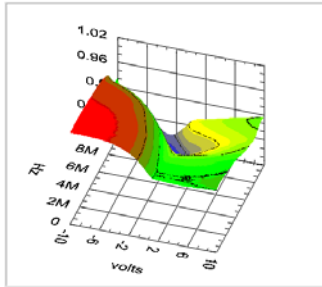


Figure 7(c)- $n_e = 7.7 \times 10^6 \text{ cm}^{-3}$

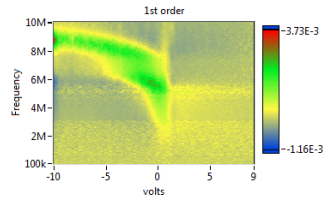
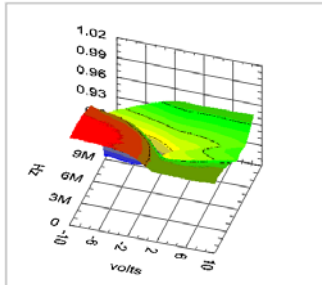


Figure 7(d)- $n_e = 2.8 \times 10^6 \text{ cm}^{-3}$

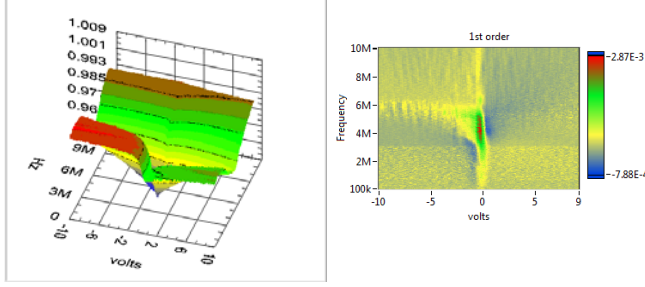


Figure 7(e)- $n_e = 1 \times 10^6 \text{ cm}^{-3}$

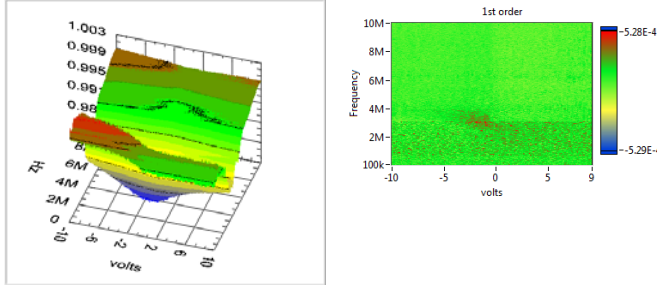


Figure 7(f)- $n_e = 2 \times 10^5 \text{ cm}^{-3}$

IV.2 Cylindrical probe

The cylindrical probe consists of a stainless steel cylinder with length, $L = 15 \text{ cm}$ and radius, $r = 0.16 \text{ cm}$ which is connected to the HP8735D Network Analyzer through 50Ω also. This arrangement including the chamber, analyzer and the coupling circuitry is shown schematically elsewhere.² The cylinder is mounted on a 1/4 inch diameter ceramic and steel support which is connected to 1/4 inch diameter semi-rigid copper 50 Ohm coaxial cable.

Figures 8(a) and 8(b) show $\text{Re}(Z_{ac})$ and $\text{Im}(Z_{ac})$ vs V_{bias} at a fixed frequency of 10 MHz for 3 different densities. In Figure 8(a) the plot of $\text{Re}(Z_{ac})$ shows the inflection point minimum as we have demonstrated earlier. In addition the minimum is seen to drift to higher plasma potentials which is also seen by a Langmuir probe. Moreover Figure 8(b) shows that $\text{Im}(Z_{ac})$ also appears to reach an inflection point at the same voltage for the different densities. Although the data show this apparent consistency our analysis is still incomplete theoretically (Refer to Eq. 14 comments and Appendix A) The applied frequency of 10 MHz for the lowest density is at the approximate boundary of the requirement that the applied frequency be less than about $f_{pe}/3$ ($f_{pe} \sim 27 \text{ MHz}$ for $n_e = 9 \times 10^6 \text{ cm}^{-3}$).

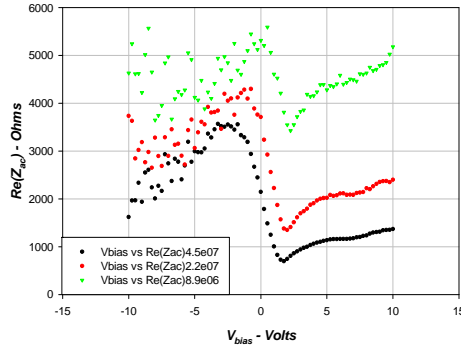


Figure 8(a)

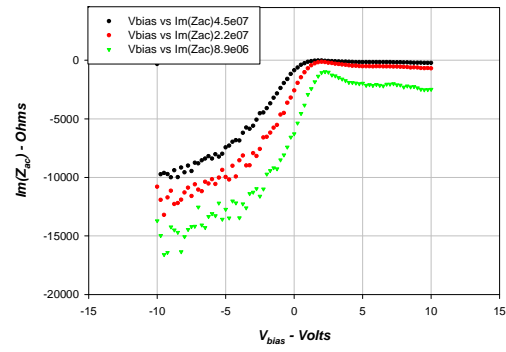


Figure 8(b)

IV.3 Disk Probe

The experiments with the disk probe were configured similarly to the cylinder and the sphere. The radius was 3.8 cm as is the 2D cross section of the sphere. Figures 9(a) and 9(b) are plots of $\text{Re}(Z_{ac})$ and $\text{Im}(Z_{ac})$ vs V_{bias} this time with varying ac frequency at a fixed density of $n_e = 4.4 \times 10^7 \text{ cm}^{-3}$. This corresponds approximately in density to Figs 6(a) and 6(b) for the sphere. We note in these plots that the minima are more distinct than in the spherical case. This is due to the fact that the disk more closely resembles an infinite plane surface where we would expect the most clearly defined inflection point

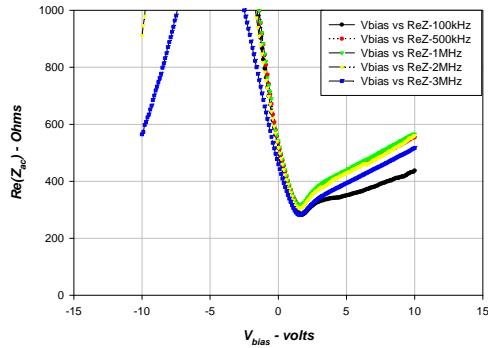


Figure 9(a)

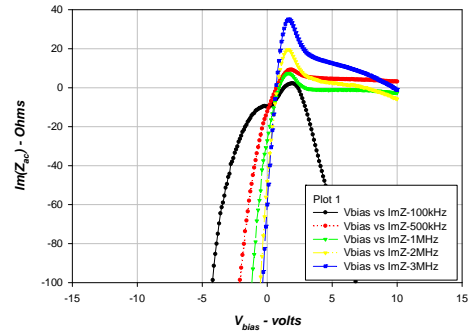


Figure 9(b)

IV.4 Comparison of Disk probe and Sphere

Figure 10 is a comparison of the disk and sphere traces for varying density. The applied signal frequency was 1 MHz. There are five plot pairs corresponding to the five densities. As mentioned above it is clear that the minima are more distinct for the disk than the sphere.

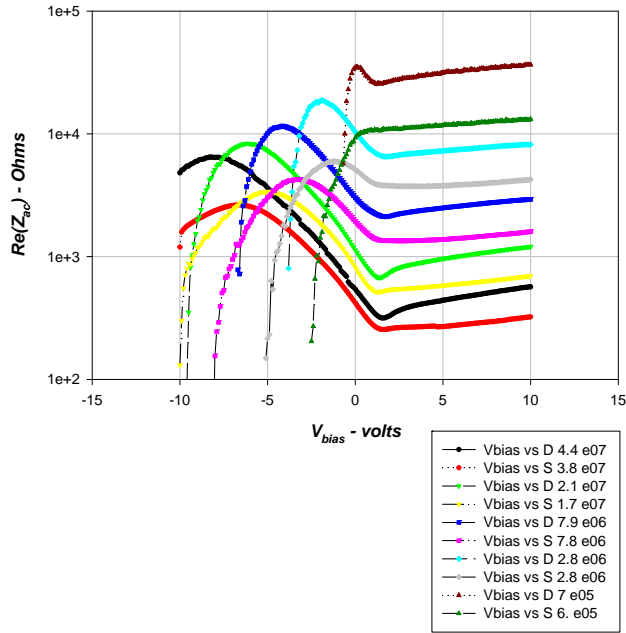


Figure 10

V. Appendix A: On $\text{Im}(Z_{ac})$ as an indicator of plasma potential

As covered in the earlier paper², the model is based on dividing the plasma into a sheath and a bulk plasma. The sheath is charged and represented by a resistor R_{ac} and sheath inductance L_{sh} both in parallel with a capacitor, C_s . The bulk plasma is assumed quasi neutral and represented in the low frequency regime by an inductance L_p . Hence, the expression for complex plasma impedance, Z , is

$$Z_{ac}(\omega) = \frac{R_{ac}[\omega^2 L_p C_s - 1] + i\omega[\omega^2 C_s L_{sh} L_p - (L_s + L_p)]}{(\omega^2 C_s L_{sh} - 1) - i\omega C_s R_{ac}} \quad \text{A.1}$$

and ,

$$\text{Re}(Z_{ac}) = \frac{R_{ac}}{(\omega^2 C_s L_{sh} - 1)^2 + (\omega C_s R_{ac})^2}, \quad \text{A.2}$$

$$\text{Im}(Z_{ac}) = \frac{[\omega^3 L_{sh} L_p C_s - \omega(L_{sh} + L_p)](\omega^2 L_{sh} C_s - 1) + \omega R_{ac}^2 C_s (\omega^2 L_p C_s - 1)}{(\omega^2 C_s L_{sh} - 1)^2 + (\omega C_s R_{ac})^2} \quad \text{A.3}$$

where C_s is the sheath ac capacitance³ and R_{ac} is the ac resistance defined above.

The inductances themselves are approximated as,

$$L_p = \int_{r_s}^{\infty} dr \frac{m_e}{4\pi r^2 e^2 n_e(r)}, \quad \text{A.4}$$

and,

$$L_{sh} = \int_{r_0}^{r_s} dr \frac{m_e}{4\pi r^2 e^2 n_{es}(r)}. \quad \text{A.5}$$

where m_e is electron mass, $n_e(r)$ is bulk plasma electron density profile from the sheath edge outward to infinity and $n_{es}(r)$ is the sheath density profile from the probe surface to the sheath edge. These expressions for spherical geometry are based on the assumption that the bulk plasma is cold and collisionless, that the current is carried by the electrons only, and that there is a slowly varying radial electric field. More detail and further assumptions necessary to approximate the inductances as above are found in the earlier works along with the solution method based on the Poisson equation. We briefly cover the relevant portions of this below.

Ignoring L_{sh} in Eq. (A.2), we find the expression for $\text{Re}(Z_{ac})$ used in Eq. 5. Also from Eq. (A.3) we have,

$$\text{Im}(Z_{ac}) = \frac{\omega L_p + \omega R_{ac}^2 C_s (\omega^2 L_p C_s - 1)}{1 + (\omega R_{ac} C_s)^2} \quad \text{A.6}$$

If, as in our assumptions allowing us to equate $\text{Re}(Z_{ac})$ to R_{ac} we assume $(\omega R_{ac} C_s)^2 \ll 1$ the derivative of $\text{Im}(Z_{ac})$ with respect to V_b , we recover Eq. 14 above,

$$\frac{\partial \text{Im}(Z_{ac})}{\partial V_b} \simeq \omega \frac{\partial L_p}{\partial V_b} - \omega R_{ac}^2 C_s \left(\frac{2}{R_{ac}} \frac{\partial R_{ac}}{\partial V_b} + \frac{1}{C_s} \frac{\partial C_s}{\partial V_b} \right) \quad \text{A.7}$$

As noted in Section IIc above, if we are able to ignore the lead term, along with the capacitance variation at plasma potential, we can conclude that the LHS of the equation vanishes along with $\partial R_{ac} / \partial V_b$. To understand when it is justifiable to ignore the lead term we rewrite Eq. (A.4),

$$L_p(V_b) = -\frac{e^{\frac{e\varphi_p}{T_e}}}{4\pi\epsilon_0\omega_{p0}^2} \int_{r_s(V_b)}^{\infty} dr \frac{e^{\frac{-e\varphi(r)}{T_e}}}{r^2} \quad \text{A.8}$$

where we have used,

$$n_e(r) = \frac{\omega_{p0}^2 \epsilon_0 m_e}{e^2} e^{\frac{e(\varphi(r)-\varphi_p)}{T_e}} \text{ with } \omega_{p0} = \left(\frac{n_{e0} e^2}{m_e \epsilon_0} \right)^{\frac{1}{2}} \quad \text{A.9}$$

with $\varphi(r)$ the potential at position r and φ_p , the plasma potential. (For an order of magnitude estimate at plasma potential, since there is no sheath,

$$L_p(\varphi_p) = \frac{1}{4\pi\epsilon_0\omega_{p0}^2 r_0} = \frac{m_e}{4\pi e^2 n_{e0} r_0}, \quad \text{A.10}$$

where $L_p(\varphi_p) \approx 1\mu\text{H}$ for $n_{e0} = 2.3 \times 10^8 \text{ cm}^{-3}$.) The derivative in the lead term now is expressed,

$$\frac{\partial L_p}{\partial V_b} = -\frac{e^{\frac{e\varphi_p}{T_e}}}{4\pi\epsilon_0\omega_{p0}^2} \int_{r_s}^{\infty} dr \left(\frac{e}{T_e} \right) \frac{\partial \varphi(r)}{\partial V_b} \frac{e^{\frac{-e\varphi(r)}{T_e}}}{r^2} \quad \text{A.11}$$

We plot $\partial L_p / \partial V_b$ after solving the integral of Eq. A.8 numerically. In this particular case the plasma potential is taken as $\varphi_p = T_e / 2e = 0.35 \text{ V}$. The first thing we notice about this plot is that the function has a minimum at approximately +0.32 volts or slightly less than φ_p . In addition, we note that the term involving this derivative in Eq. A.7 is multiplied by ω . So clearly the lower the applied frequency, the better the approximation to neglect the leading term becomes independently of whether it reaches a minimum at φ_p . i.e., if the term is small enough to ignore, its behavior is irrelevant. (put correct scale values in this plot)..

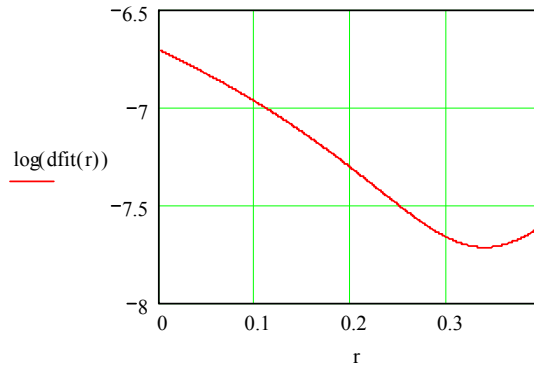


Figure A.1

Finally we plot the theoretical dependence of $\text{Im}(Z_{ac})$ on density in Figure A.2. Since as yet our model is not complete in terms of behavior of the collected current past φ_p in the case where the sheath is very thin compared to probe dimensions, we terminate the data just before $\varphi_p = T_e / 2e = 0.35 \text{ V}$. The Figure appears to show $\text{Im}(Z_{ac})$ tending toward a road maximum but this is not well-defined and certainly not as clear a

maximum as is indicated in the data. However, the dependence of the curves on density is observed experimentally and our solution, although not complete, shows predicted behavior consistent with observation.

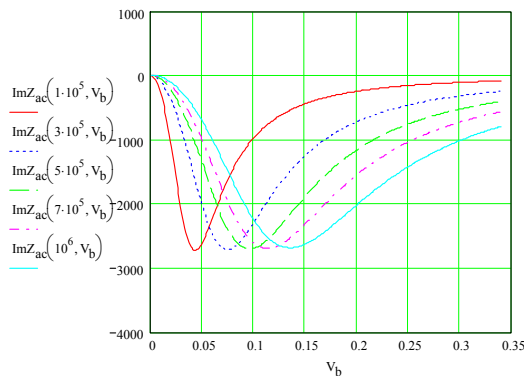


Figure A.2

Finally, it should be noted that or larger sheaths as mentioned L_{sh} can become quite large and we are out of the area of validity of the thin sheath model for most, but not all, cases. This can be studied further.

VI. Summary

We have performed experiments in low electron density and temperature plasma to determine the effect on measurements of plasma potential using an algorithm for which we hold a US patent. We have added to that basic method 3 additional indicators of plasma potential using both $\text{Im}(Z_{ac})$ and the reflection coefficient, Γ , and their derivatives. Although experimentally seen as reaching a maximum at (or near) plasma potential, present theory is not complete in justifying this observation. The results are consistent with alternate methods such Langmuir and emissive probe measurements. The new indicators are most useful in low density plasma where it is often difficult to isolate plasma potential.

VII. References:

- ¹D.N. Walker, R.F. Fernsler, D.D. Blackwell, W.E. Amatucci, and S.J. Messer, *Phys. Plasmas* **13**, 032108 (2006)
- ²D.N. Walker, R.F. Fernsler, D.D. Blackwell, W.E. Amatucci, *Phys. Plasmas* **15**, 123506 (2008)
- ³D.N. Walker, R.F. Fernsler, D.D. Blackwell, W.E. Amatucci, *Phys. Plasmas* **17**, 113503 (2010)
- ⁴D.N. Walker, R.F. Fernsler, D.D. Blackwell, W.E. Amatucci, *NRL Memorandum Report*, **6750-11-9331** (2011)
- ⁵F.F. Chen, Electric Probes, *Plasma Diagnostic Techniques*, R.H. Huddleston and S.L. Leonard (Ed.), (Academic, NY, 1965)
- ⁶R.L. Merlino, *Am. J. Phys.*, **75**, 12, 1078, 2007
- ⁷J.G. Laframboise, (PhD Thesis) Univ. of Toronto, *Institute for Aerospace Studies, Report No. 100*, (1966)
- ⁸R.F. Fernsler, *Plasma Sources Sci. and Technol*, **18**, 014012 (2009)